New Insight From the First Application of Ti-in-Quartz (TitaniQ) Thermometry Mapping in the Eastern Khondalite Belt, North China Craton

Yuanyuan Zheng [1,2,3], Yang Qi [1,2,3], Di Zhang [1,2], Shujuan Jiao [1,2]*, Guangyu Huang [1,2] and Jinghui Guo [1,2]

[1]State Key Laboratory of Lithospheric Evolution, Institute of Geology and Geophysics, Chinese Academy of Sciences, Beijing, China, [2]Innovation Academy for Earth Science, CAS, Beijing, China, [3]College of Earth and Planetary Sciences, University of Chinese Academy of Sciences, Beijing, China

The thermal regime of the lower crust is a critical factor that controls crustal anatexis, high-grade metamorphism, and granite formation, which finally results in crustal differentiation. However, the large-scale thermal regime in the Precambrian continental crust is generally not well established. In this study, we first applied Ti-in-quartz (TitaniQ) thermometer to map the temperature variation in the lower crust within an area of ~10,000 km^2 in the Paleoproterozoic eastern Khondalite Belt, North China Craton. The studied rocks are aluminous gneisses/granulites, which contain abundant quartz that generally coexists with rutile. The results show that matrix-type quartz with substantial rutile exsolution generally contains the maximum Ti concentration, which is <300 ppm higher than that of inclusion-type quartz. This result suggests that two quartz types probably formed at the prograde and near-peak to early cooling metamorphic stages, respectively. Therefore, the temperature mapping result based on the maximum Ti concentrations of the matrix-type quartz can better represent the thermal regime than inclusion-type quartz. Our regime shows that the hottest Paleoproterozoic lower crust is underneath the Liangcheng-Heling'er-Zhuozi area, where ultrahigh-temperature (UHT) metamorphism is closely associated with abundant charnockite. The hottest region may represent the root of an ancient large hot orogeny. Our study provides a new insight into the formation of UHT metamorphism.

Keywords: Ti-in-quartz (TitaniQ) thermometer, aluminous gneiss/granulite, UHT metamorphism, thermal regime, the khondalite belt, North China Craton

INTRODUCTION

Ultrahigh-temperature (UHT) metamorphism occurs at temperatures of ≥900°C (0.7–1.3 GPa; Harley, 1998), and is the hottest metamorphism in the lower crust. The first UHT metamorphism was reported over 50 years ago. Numbers of UHT localities have been discovered worldwide, and detailed studies have laid the foundation for a complete understanding of the crustal thermal regime (Harley, 1998; Sajeev et al., 2004; Santosh et al., 2007a; Harley, 2008; Janwari et al., 2012). Study of UHT metamorphism facilitates interpreting the lithospheric evolution throughout Earth's history, especially the crust–mantle interaction and tectonic evolution.

The Khondalite Belt within the North China Craton (NCC) was formed by the collision of the Yinshan Block in the north and the Ordos Block in the south at ca. 1.95 Ga (Zhao et al., 2005). Since the first identification of two typical UHT metamorphic localities at Dongpo in the Daqingshan terrane (Guo et al., 2012) and Tuguiwula in the Jining terrane (Santosh et al., 2006), investigations have discovered new localities of UHT rocks, for example, Tuguishan, Xuwujia, Hongsigou, Zhaojiayao, Xumayao, Nantianmen, and Xiaonangou (Jiao et al., 2011; Jiao and Guo, 2011; Liu et al., 2012; Zhang et al., 2012; Yang et al., 2014; Li and Wei, 2016; Wang et al., 2020). However, their spatial relationship, especially the distribution area of UHT metamorphism, is ambiguous.

Numerous methods have been applied to estimate the peak metamorphic temperature of UHT granulites, including thermometers and phase equilibria modeling. The thermometers of two-feldspar, Zr-in-rutile, Ti-in-zircon, and Al-in-orthopyroxene performed well in the UHT temperature estimates. Titanium in quartz was also calibrated as a Ti-in-quartz (TitaniQ) thermometer (Ostapenko et al., 1987; Wark and Watson, 2006; Thomas et al., 2010; Huang and Audétat, 2012; Zhang et al., 2020), which has been applied to various rock types and proved to be valid (Spear and Wark, 2009; Storm and Spear, 2009; Thomas and Bruce Watson, 2012; Kidder et al., 2013; Tual et al., 2018). Quartz is ubiquitous in many UHT rocks, and the application of the TitaniQ thermometer is convenient because only the quartz phase needs to be analyzed. In addition, quartz internal structures revealed by cathodoluminescence (CL) images can assist in interpreting the mechanism of quartz formation (Sprunt et al., 1978; Müller et al., 2002; Kendrick and Indares, 2018). Therefore, the application of the TitaniQ thermometer in combination with quartz CL imaging can potentially indicate the metamorphic evolution of UHT granulites.

In this study, we applied the TitaniQ thermometer and CL imaging of quartz to metapelites (including UHT granulites) in the eastern Khondalite Belt for the first time. The samples were collected from an area of ~10,000 km^2 to conduct regional temperature mapping. Our approach provides a new simple method for calculating metamorphic temperature in this region. Our temperature mapping shows the regional thermal regime of the lower crust and provides a new insight into the formation of UHT metamorphism.

GEOLOGICAL SETTING AND SAMPLING LOCALITY

The formation and evolution of the NCC have been topics of ongoing debates for many decades. As the oldest craton in China with an age record of up to 3.8 Ga (Liu et al., 1992; Wan et al., 2005), the NCC has experienced complicated geological processes. The model ages from zircon Hf isotope and whole-rock Nd isotope in TTG gneisses suggest that the formation age of the continental crust of NCC is 2.8–2.7 Ga and ca. 2.5 Ga (Wu et al., 2005; Geng et al., 2012).

A suggestion has been that the NCC could be divided into three major tectonic units: The Western block, the Eastern block,
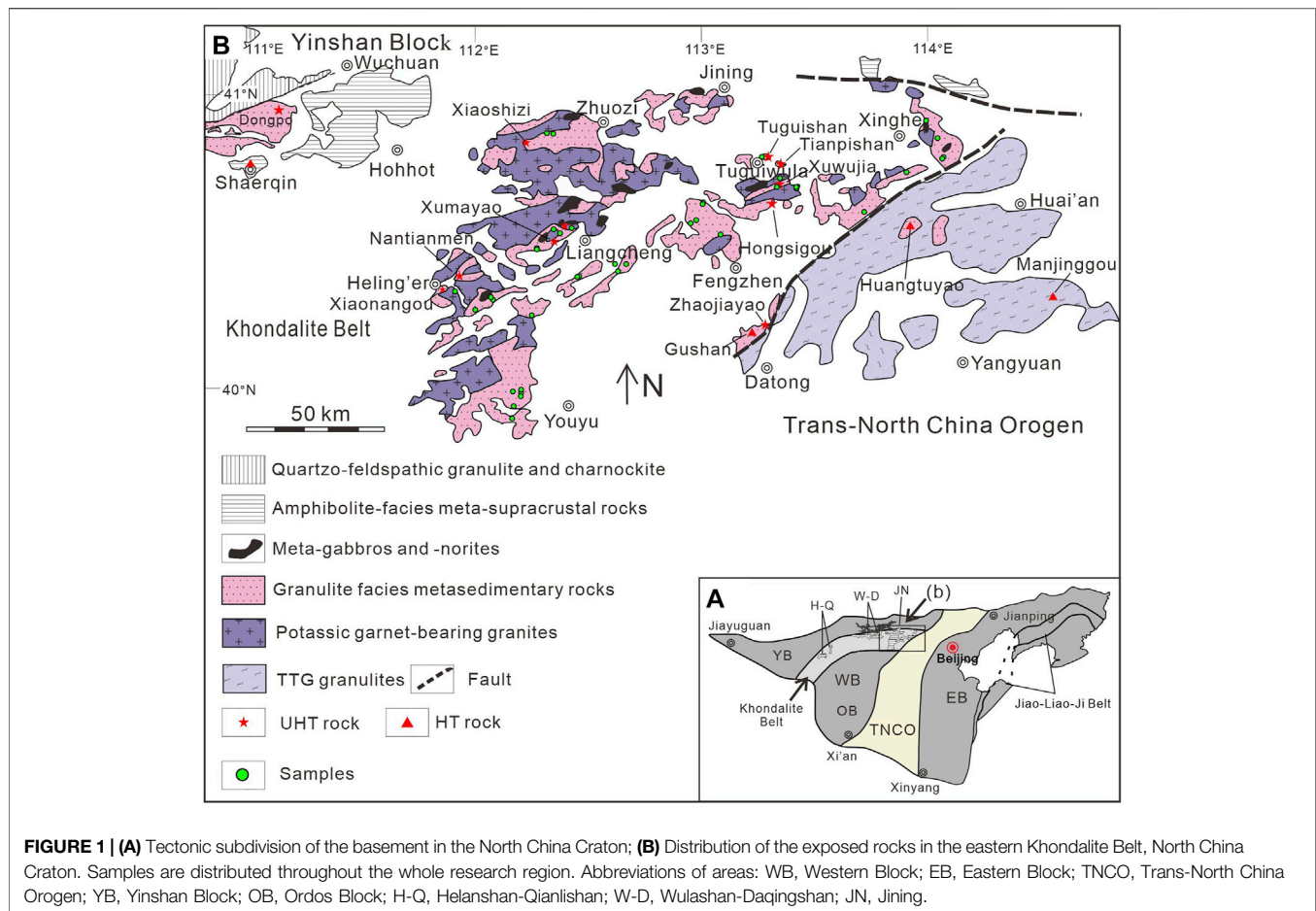
and the collisional belt of the Trans-North China Orogen (Zhao et al., 2011). There are two other recognized orogens: the Jiao-Liao-Ji Belt in the Eastern Block, formed by the collision between the Nangrim Block and Longgang Block at ca. 1.95–1.90 Ga and the Khondalite Belt in the Western Block, formed by the collision between the Yinshan Block and Ordos Block at ca. 1.95 Ga, which is related to the assembly of the Columbia supercontinent (Zhao et al., 1998; Zhao et al., 2001; Zhao et al., 2003; Zhao et al., 2005; Zhao et al., 2011).

The east-west trending Khondalite Belt is located in the north-central part of the Western Block, NCC. It can be divided into three terranes from west to east: Helanshan-Qianlishan (H-Q), Wulashan-Daqingshan (W-D), and Jining (JN) terranes (**Figure 1A**). The rock types of the belt are composed of khondalite series rocks (aluminum-rich meta-sedimentary rocks), garnet-cordierite granites, charnockites, meta-gabbros, and a small amount of TTG gneisses. Zircon geochronological results suggest that detrital materials in the Khondalite Belt were derived from Archean and Paleoproterozoic magmatism (Zhai and Peng, 2007; Zhai, 2009). The protolith of the Khondalite series is considered to have been deposited between 2.00 and 1.95 Ga, which represents the deposition of an active continent margin, instead of an Archean cratonic basin (Wan et al., 2009; Dan et al., 2012).

The whole Khondalite Belt has experienced upper amphibolite- to granulite-facies metamorphism, including high-pressure metamorphism between 1.96 and 1.94 Ga and an overprinted HT-UHT metamorphism event at 1.94–1.80 Ga (Santosh et al., 2007b; Santosh et al., 2009; Yin et al., 2011; Jiao et al., 2020; Jiao and Guo, 2020; Jiao et al., 2021).

In the Helanshan-Qianlishan terrane of western Khondalite Belt, the calculated peak temperature and pressure conditions are 850–870°C and 1.4–1.5 GPa, within a clockwise P–T path, and this high-pressure metamorphism suggests the occurrence of continent-continent collision in the Khondalite Belt (Yin et al., 2009; Yin et al., 2011; Yin et al., 2015; Zhou et al., 2010). In the Wulashan-Daqingshan terrane, rock types are variable and contain meta-sedimentary rocks, Archean TTG gneisses, and mafic granulites, with varying degrees of multi-metamorphism (Jiang et al., 2022).

Rock types in the Jining terrane of eastern Khondalite Belt are khondalite series rocks associated with a small amount of quartzite, graphite gneiss, marble, calc-siliceous gneiss, potassic garnet-bearing granite, and intrusive meta-gabbro and –norite (**Figure 1B**). The distribution area of the potassic garnet-bearing granite is large: 40% of the rock exposed (**Figure 1A**). The potassic garnet-bearing granite is dominated by abundant charnockite associated with minor leucogranites, which represent two periods of magmatic events (Peng et al., 2012; Wang et al., 2017; Wang et al., 2018). The distribution area of intrusive meta-gabbros and norites is small. A suggestion has been that the formation of meta-gabbros and meta-norites provides a heat source for UHT metamorphism (Peng et al., 2010; Peng et al., 2012), which leads to the formation of garnet-bearing granite by *in-situ* anatexis of khondalite series rocks. The volume of granites is one third to one half of the khondalite series rocks, and the age

FIGURE 1 | (A) Tectonic subdivision of the basement in the North China Craton; **(B)** Distribution of the exposed rocks in the eastern Khondalite Belt, North China Craton. Samples are distributed throughout the whole research region. Abbreviations of areas: WB, Western Block; EB, Eastern Block; TNCO, Trans-North China Orogen; YB, Yinshan Block; OB, Ordos Block; H-Q, Helanshan-Qianlishan; W-D, Wulashan-Daqingshan; JN, Jining.

of granite formation is coeval with the metamorphic age of khondalite series rocks (Zhai, 2009).

Sapphirine-bearing metapelites or residual granulites have been discovered at the Dongpo and Shaerqin localities in the Wulashan-Daqingshan terrane, recording HT-UHT conditions of 910–980°C and 860–890°C, respectively (Guo et al., 2012; Jiao et al., 2015). The sapphirine-bearing UHT granulites were reported from the Tuguiwula (Tianpishan) locality (Santosh et al., 2007a), which preserves the diagnostic UHT mineral assemblages of Spr + Qz and Opx + Sil + Qz (Mineral abbreviations follow Warr, 2021), and the near-peak temperature of 900–1,000°C was recorded. Subsequently, additional UHT granulite localities have been reported in the Jining terrane, such as Tuguishan, Xuwujia, Nantianmen, Xiaonangou, and Xumayao (Santosh et al., 2007a; Jiao et al., 2011; Jiao and Guo, 2011; Liu et al., 2012; Zhang et al., 2012). In Helanshan terrane, UHT metamorphism was reported in spinel-bearing granulites, with peak conditions of ∼ 960–1,030°C and 6.3–7.3 kbar (Gou et al., 2018). Generally, the UHT granulites in the Khondalite Belt have experienced complex clockwise *P–T* paths, including decompression-heating, nearly isobaric cooling (IBC), and nearly isothermal decompression/decompression-heating stages, although anticlockwise *P–T* paths were also proposed (**Figure 2**; Liu et al., 2010; Jiao et al., 2011; Jiao and Guo, 2011; Li and Wei, 2016).

Our research region is the Jining-Tuguiwula-Liangcheng-Heling'er-Youyu area located within the Jining terrane of the eastern Khondalite Belt (**Figure 1B**), which contains several UHT localities. Forty-four representative samples throughout this region were studied using a TitaniQ thermometer to constrain the occurrence and spatial scale of the UHT metamorphism.

PETROGRAPHY

The studied samples were mostly aluminous gneisses (or granulites). The major minerals in these samples are quartz, plagioclase, K-feldspar, garnet, sillimanite, and biotite. These samples were classified into four groups. The first group is characterized by a Grt + Sil + Bt + Qz + Pl/Kfs mineral assemblage, which can be subdivided into coarse-grained and fine-grained according to the granularity of garnet grains (**Figures 3A,B**). Thirty-two samples belong to this group, accounting for the majority of the samples. In addition, four samples in this group had distinct foliation structures (samples 20HL19, 20HL39, 20HL89, 20HL143) (**Figure 3C**). The oriented arrangement of sillimanite composes the foliation. Except for sillimanite, minerals such as quartz, biotite, and resorbed garnet can also compose the foliation. The second group was

characterized by a Grt + Bt + Qz + Pl/Kfs mineral assemblage and comprised four samples (**Figure 3D**). In this group, the volume proportion of sillimanite was relatively low to none, and biotite was the main aluminous-rich mineral. The third group was characterized by a Grt + Sil + Qz + Pl/Kfs mineral assemblage and comprised three samples (**Figure 3E**). In this group, the size of the biotite was small, and the main aluminous-rich mineral was sillimanite. The fourth group was characterized by a Grt + Qz + Pl/Kfs mineral assemblage and comprised five samples (**Figure 3F**).

Garnet occurs as porphyroblasts in all samples, which contain quartz, plagioclase, biotite, and rutile as inclusions. Garnet in some samples had been resorbed and broken into small pieces. Plagioclase and K-feldspar are commonly present in the matrix. K-feldspar had been altered in some samples. Sillimanite mainly occurs in the matrix in the needle-and-column shape. Lamellar biotite mainly disperses in the matrix: Some grains are distributed around garnet, and some occur as inclusions in garnet. Quartz exists in two forms: Matrix-type quartz and quartz inclusions in garnet. In some samples, rutile needles are within quartz grains, which can be observed in the photomicrographs. In some samples, rutile grew along three directions, which may represent the crystallization direction. We observed that the occurrence of rutile needles in quartz grains from the northern part is more general than that in the southern part of the studied region.

Rutile exists as an accessory phase in all the samples. Most of the rutile grains occur in the matrix surrounded by quartz, and the others occur as inclusions in garnet. The volume proportion and grain size of rutile differ. In five samples from south of Heling'er (samples 20HL49, 20HL59, 20HL64, 20HL73, and 20HL89), rutile was 50–200 μm in size and had an extremely low volume percentage. By contrast, rutile in samples from the Xinghe area was 100–800 μm and occupied a higher volume percentage (samples 09XH07, 09XH16, 09XH21, and 09XH32). In samples from Tuguishan locality, a few spinel grains with grain sizes of 100–250 μm were observed (samples 09TGS01, 09TGS18, and 18TG01), which is distinct from the other samples.

ANALYTICAL METHODS

Electron Microprobe Analysis

Concentrations of major (Si) and minor (Al and Ti) elements in quartz grains were all determined by CAMECA SXFive electron probe micro-analyzer at the Institute of Geology and Geophysics, Chinese Academy of Sciences (IGGCAS) in Beijing, China. Accelerating voltage was 15 kV and beam currents were 30 and 300 nA for major and minor elements. The peak counting times were 20s for Si and 120s for Al and Ti. Rhodonite, albite and rutile were used as standards for calibration. Standardization was performed with a beam current of 20 nA and with a peak counting time of 20s. Data were obtained by the X-PHI matrix correction (Merlet, 1994). Oxygen was calculated by cation stoichiometry and included in the matrix correction. The following detection limits were based on a 3σ estimate of the measured background variance: ~210 ppm for Si, ~12 ppm for Al and ~13 ppm for Ti.

A large spot size of 50 μm was used for all analyses in order to involve the composition of substantial rutile needles in the measurement, because TiO_2 in these rutile needles might have once occupied by pre-existing quartz that is before rutile exsolution (See *Section Discussion*). The natural smoky quartz crystal was used as a secondary standard, which has reproducible Ti concentration (57 ± 4 ppm; Audétat et al., 2015). Our averaged Ti concentration (N = 55) of the quartz standard is 58 ± 3 ppm, which is consistent with the recommended value within error. Our analyzed quartz grains in the matrix are all far away from other major Ti-bearing minerals, such as rutile and biotite, to avoid secondary fluorescence effect.
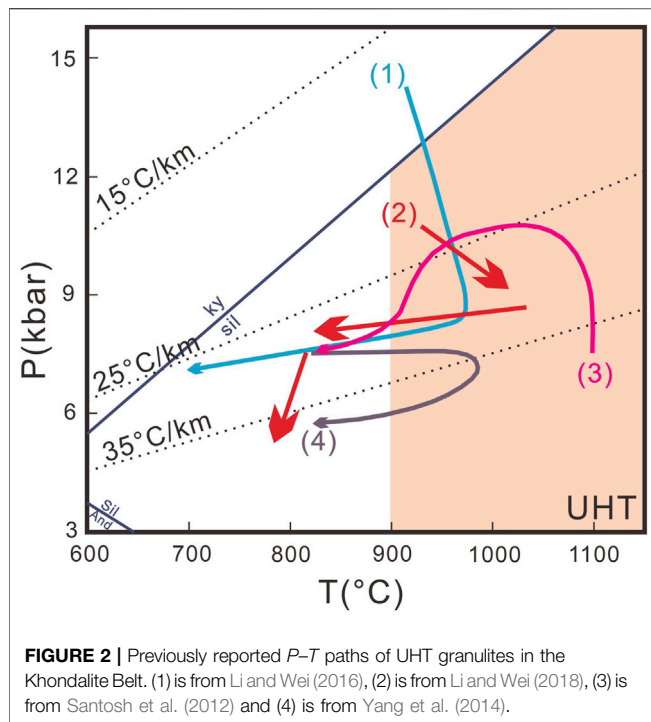
Cathodoluminescence Imaging

The Cathodoluminescence (CL) images of quartz were observed using a Nova NanoSEM 450 (FSEM) scanning electron microscope at the IGGCAS. The Nova NanoSEM 450 was equipped with a Gatan Instrument "MonoCL14" detector. An accelerating voltage of 10 kV and a beam current of 1.1 nA were used during the analysis, and the working distance was 27–29 mm.

Thermometry

The titanium concentration in quartz was first proposed as a geological thermometer in 1987 (Ostapenko et al., 1987). The thermodynamic principle of the TitaniQ thermometer depends on the titanium equilibrium between quartz and rutile, which can be expressed in an exchange reaction: $TiO_2^{Qz} = TiO_2^{Rt}$. The calibration experiments suggest that titanium solubility in quartz depends on the pressure and temperature conditions in the case that quartz crystallizes coexisting with rutile, and titanium contents of quartz (in ppm by weight) would increase exponentially with T. Similar to other trace-element thermometers, TitaniQ thermometer has several calibrations (Wark and Watson, 2006; Thomas et al., 2010; Huang and Audétat, 2012; Thomas et al., 2015). Within these models, the experiments were set to high pressure (5–20 kbar) and high temperature (700–940°C) conditions in the Thomas et al. (2010) model, which is the most suitable for the metamorphic conditions of our studied samples. Hence, we used the model calibrated by Thomas et al. (Thomas et al., 2010) in this study. And the pressure we have chosen for all calculations is 8 kbar based on couples of previous studies in the eastern Khondalite Belt (**Figure 2**; e.g., Santosh et al., 2007a; Santosh et al., 2012; Jiao et al., 2013a; Yang et al., 2014; Li and Wei, 2016; Li and Wei, 2018).

When applying the TitaniQ thermometer, the activity of TiO_2 should be accurately estimated. The value is generally 1 if rutile exists in the studied rocks, which means that the system is TiO_2 saturated (Ghent and Stout, 1984). There are also methods for calculating TiO_2 activity if the rocks do not contain rutile, which are mainly based on different solution models and compositions of Fe-Ti oxides (Hayden and Watson, 2007; Hildreth and Wilson, 2007; Kularatne and Audétat, 2014).

FIGURE 2 | Previously reported *P–T* paths of UHT granulites in the Khondalite Belt. (1) is from Li and Wei (2016), (2) is from Li and Wei (2018), (3) is from Santosh et al. (2012) and (4) is from Yang et al. (2014).

All samples in this study contain rutile, although the grain size and volume percentage vary. For example, five samples from south of Heling'er (samples 20HL49, 20HL59, 20HL64, 20HL73, and 20HL89) contain few tiny rutile. A study suggested that fluid remains saturated with respect to rutile once the fluid is rutile-saturated, and subsequent rutile growth is not sufficient to drive the liquid to rutile-undersaturation (Acosta et al., 2020). Although the absence of rutile does not necessarily imply quartz growth from a rutile-undersaturated liquid, researcher interpreted it as a liquid that was near saturation but below the critical supersaturation required to nucleate new rutile crystals (Acosta et al., 2020). Because of the aforementioned reasons, we used a TiO_2 activity of 1 for all samples.

TitaniQ temperature mapping was conducted using ArcGIS with the inverse distance weighted interpolation method.

RESULT

Quartz Ti Concentrations and Temperatures by TitaniQ

A total of 463 spots were analyzed in 44 samples. Analyses with unacceptable total SiO_2 content (>105 or <95) were discarded. We finally obtained 417 valid data points (**Supplementary Tables S1, S2**), among which 182 were quartz inclusions within garnet from 42 samples (**Supplementary Table S1**), and 235 were of matrix-type quartz from 43 samples (**Supplementary Table S2**).

Within quartz inclusions of garnet, Ti concentrations range from 40 to 550 ppm. We calculated the average Ti concentrations for each sample, which range from 58 to 420 ppm, and four data points of extremely high Ti concentrations far from the others

within several samples (samples 20HL34, 20HL59, 20HL64, and 09TGS01) were not included and regarded as outlier data (**Figure 3A**). Temperatures calculated by the TitaniQ thermometer for these quartz average Ti concentrations range from 654°C (sample 20HL89) to 891°C (sample 18LC01), all below UHT conditions (**Figure 4A**). The maximum Ti concentrations of each sample range from 65 to 550 ppm, the corresponding TitaniQ temperatures range from 665 to 934°C, and the highest temperatures are from samples in the Liangcheng and Zhuozi areas (**Figure 4B**).

Within matrix-type quartz, Ti concentrations range from 30 to 1,000 ppm. The calculated average Ti concentrations for each sample, range from 100 to 528 ppm, and six data points of extremely high Ti concentrations far from the others within several samples (i.e., samples 18ZZ01, 20HL104, 18TG01, 18TG04, and 09XH32) were not included, and were regarded as outlier data (**Figure 4C**). Temperatures calculated by the TitaniQ thermometer for these quartz average Ti concentrations range from 685 to 917°C (**Figure 4D**), and some of them have recorded UHT metamorphic conditions. The maximum Ti concentrations of each sample range from 156 to 680 ppm (**Figure 4C**), and the corresponding TitaniQ temperatures are 760–970°C, and the highest temperatures are also from samples in the Liangcheng and Zhuozi areas (**Figure 4D**).

We compared the difference in average Ti concentrations between the matrix-type quartz and quartz inclusions for each sample, without considering the outlier data (**Figure 5A**). The matrix-type quartz contains Ti concentrations <180 ppm higher than that of quartz inclusions, and only five samples show an inverse trend (**Figure 5A**). Therefore, the temperature calculated for the matrix-type quartz is generally <120°C higher than that of quartz inclusions (**Figure 5B**).

We also compared the difference in maximum Ti concentrations between the matrix-type quartz and quartz inclusions for each sample, without considering the outlier data (**Figure 5C**). The matrix-type quartz also contains Ti concentrations <300 ppm higher than that of quartz inclusions. The temperature calculated for matrix-type quartz is generally <160°C higher than that of quartz inclusions (**Figure 5D**).

Quartz Internal Structures

The CL images revealed types of quartz internal structures not observed in the photomicrographs. We divided quartz according to internal structure into four types: 1) Non-structure with homogeneous luminescence, 2) linear structure with low luminescence, 3) sealed fractures, and 4) reticular structures.

The non-structure with homogeneous luminescence is the simplest CL image in our samples and displays uniform luminescence without a special structure (**Figure 6**). It is more common in quartz inclusions than in matrix-type quartz. Quartz inclusions with non-structure contain low Ti concentrations, generally 100–200 ppm, and TitaniQ temperatures are 700–800°C (**Figures 6A,B**). Matrix-type quartz with non-structure has different Ti concentrations, which could be as low as 225 ppm with a TitaniQ temperature of 805°C
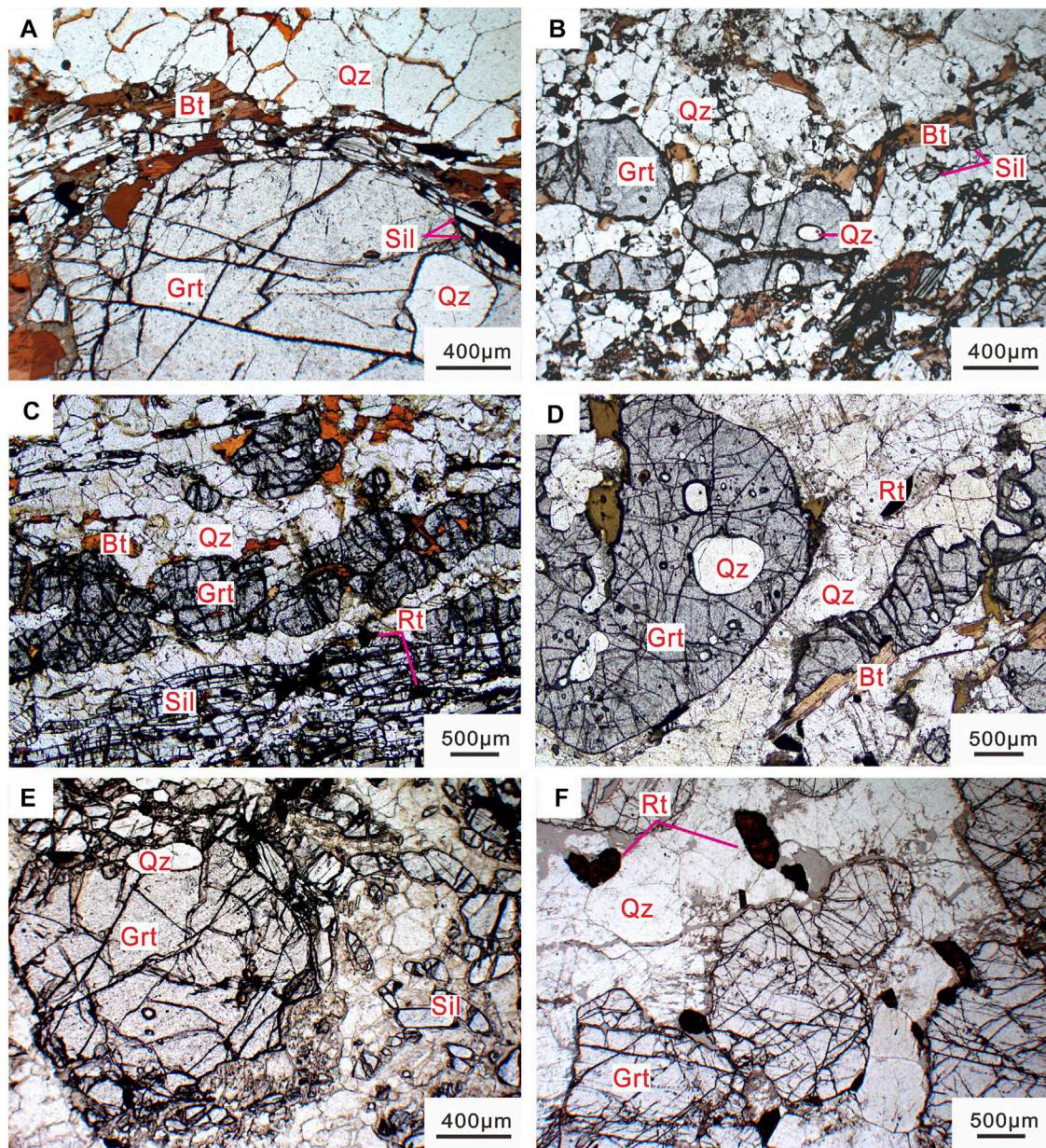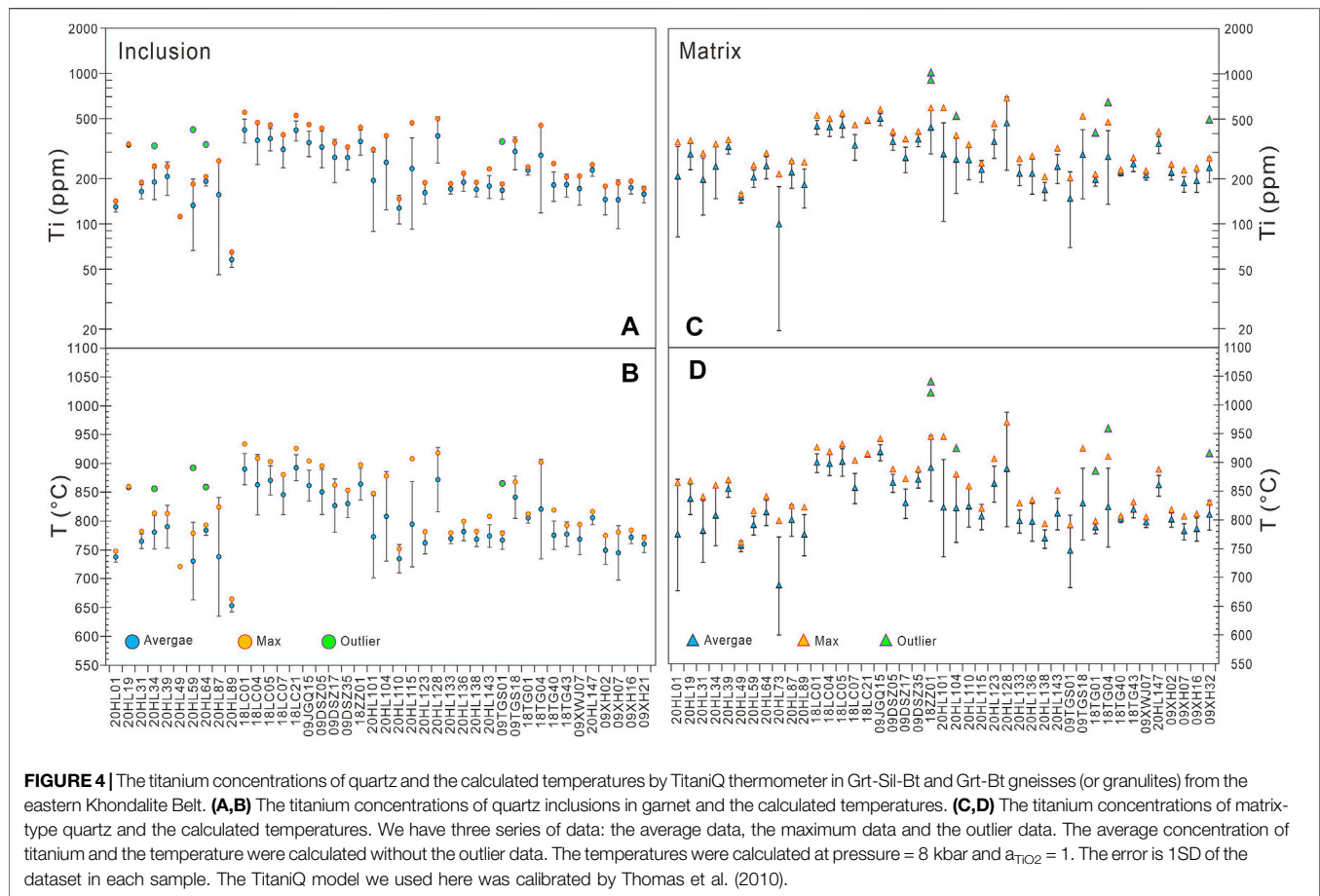
FIGURE 3 | Photomicrographs showing the typical mineral assemblages and quartz micro-textures of samples from the eastern Khondalite Belt, North China Craton. **(A)** Quartz occurs as inclusions in rims of coarse-grained garnet, and in the matrix from Grt-Sil-Bt gneiss (sample 20HL64); **(B)** Quartz is included by fine-grained garnet and occurs in the matrix from Grt-Sil-Bt gneiss (sample 20HL39); **(C)** Quartz occurs in the matrix from fine-grained Grt-Sil-Bt gneiss (sample 20HL19), the oriented arrangement of sillimanite defines the foliation; **(D)** Quartz occurs as inclusions in rims of coarse-grained garnet, and in the matrix from Grt-Bt gneiss/granulite (sample 18LC21), with rutile in the matrix; **(E)** Quartz occurs as inclusions in rim of coarse-grained garnet, and in the matrix from Grt-Sil gneiss (sample 20HL123); **(F)** Garnet occurs as porphyroblast with quartz and rutile in the matrix from garnet-bearing gneiss/granulite (sample 09XH21). Mineral abbreviations follow Warr (2021).

(**Figure 6D**) and as high as 490 ppm with a TitaniQ temperature of 917°C (**Figure 6F**).

A linear structure with low luminescence occurs in both quartz inclusions and matrix-type quartz (**Figure 7**). These dark linearities within quartz generally correspond to the rutile needles shown in the photomicrographs. Rutile is rare and barely visible under photomicrographs but distinct in CL images. The occurrence of rutile needles is more common in

quartz inclusions than in matrix-type quartz but generally occurs in the cores of the grains. Quartz Ti concentrations within rutile needle-rich domains are commonly high (>250 ppm), and the corresponding temperatures are >820°C (**Figure 7**).

Healed fractures characterized by healed microcracks and dark patches occur in both quartz inclusions and matrix-type quartz (**Figure 8**). The dark patches grew around and extended along the cracks. Healed fractures generally occur simultaneously with

FIGURE 4 | The titanium concentrations of quartz and the calculated temperatures by TitaniQ thermometer in Grt-Sil-Bt and Grt-Bt gneisses (or granulites) from the eastern Khondalite Belt. **(A,B)** The titanium concentrations of quartz inclusions in garnet and the calculated temperatures. **(C,D)** The titanium concentrations of matrix-type quartz and the calculated temperatures. We have three series of data: the average data, the maximum data and the outlier data. The average concentration of titanium and the temperature were calculated without the outlier data. The temperatures were calculated at pressure = 8 kbar and a_{TiO2} = 1. The error is 1SD of the dataset in each sample. The TitaniQ model we used here was calibrated by Thomas et al. (2010).

rutile needles (i.e., linear structures with low luminescence). Thus, quartz with healed fractures also has high Ti concentrations of >200 ppm and corresponding temperatures of >790°C (**Figures 8B,D**).

Reticular structures only occur in a few quartz grains (**Figure 9**). An irregular pattern of differential CL forms an enigmatic reticular microstructure. It is likely that a large single quartz crystal with bright luminescence is separated by dark stringers into numerous sub-crystals. However, this structure occurs differently in quartz inclusions and matrix-type quartz; in the former, the dark stringers are relatively blurry and disappear in the rim of the grain (**Figure 9B**). By contrast, the stringers are more fully developed in the matrix-type quartz (**Figure 9D**). Quartz grains with this internal structure generally contain low Ti concentrations of <250 ppm and corresponding temperatures of <820°C (**Figure 9**).
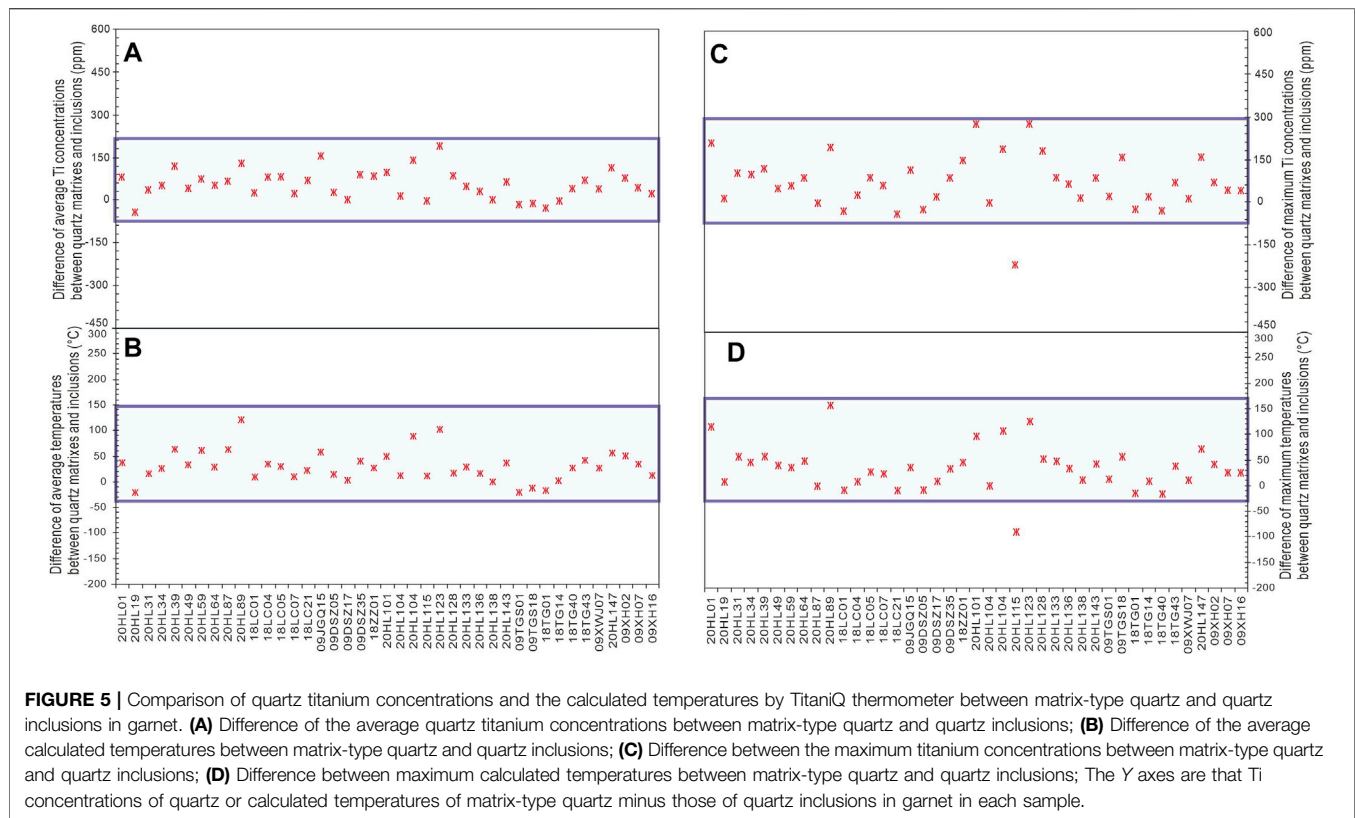
DISCUSSION

Multi-Stage Quartz Formation/Alteration During Metamorphism

Studies have constrained the metamorphic age and *P–T* path of aluminous gneisses/granulites in the eastern Khondalite Belt.

Zircon U-Pb dating and detailed petrological investigations in combination with phase equilibria modeling have constrained the timing of UHT metamorphism at 1.94–1.80 Ga, following the prior HP metamorphism (Santosh et al., 2007b; Jiao et al., 2013b; Li and Wei, 2016). The *P–T* paths involved post-peak cooling and decompression stages, although the prograde stages were variable (**Figure 2**; Santosh et al., 2007a; Santosh et al., 2012; Yang et al., 2014; Li and Wei, 2016; Li and Wei, 2018). We interpret the quartz formation based on the aforementioned metamorphic evolution history.

Quartz inclusions in garnet generally contain less Ti concentrations than matrix-type quartz, and the TitaniQ temperature is <160°C lower (**Figure 5**). This result suggests that the quartz inclusions probably grew during prograde metamorphism. Garnet may protect quartz inclusions from later resetting. However, quartz inclusions have a wide range of Ti concentrations, which may represent quartz inclusions that formed during different periods of prograde metamorphism, or are reset by later retrogression. Quartz inclusions with homogeneous luminescence CL images have low Ti concentrations, which may form at relatively low temperatures during the early prograde period, and others with rutile needles have high Ti concentrations and may form at relatively higher temperature conditions of the prograde metamorphism.

FIGURE 5 | Comparison of quartz titanium concentrations and the calculated temperatures by TitaniQ thermometer between matrix-type quartz and quartz inclusions in garnet. **(A)** Difference of the average quartz titanium concentrations between matrix-type quartz and quartz inclusions; **(B)** Difference of the average calculated temperatures between matrix-type quartz and quartz inclusions; **(C)** Difference between the maximum titanium concentrations between matrix-type quartz and quartz inclusions; **(D)** Difference between maximum calculated temperatures between matrix-type quartz and quartz inclusions; The *Y* axes are that Ti concentrations of quartz or calculated temperatures of matrix-type quartz minus those of quartz inclusions in garnet in each sample.

Matrix-type quartz was dominant in the studied rocks. The grains with homogeneous luminescence CL images and rutile needle structures that contain high Ti concentrations probably formed during the near-peak or early cooling stage. It was suggested that the high-temperature quartz that crystallized from the residual melt during early cooling is characterized by non-structure homogeneous luminescence CL (Storm and Spear, 2009).

The occurrence of rutile needles has been observed in Ti-rich quartz interiors of medium- to high-grade metamorphic rocks, such as quartz in migmatites and UHT metamorphic rocks (Cherniak et al., 2007; Sato and Santosh, 2007; Storm and Spear, 2009). Two mechanisms have been proposed to explain these features: 1) The entrapment of preexisting acicular rutile by growing quartz and 2) the exsolution of high-Ti quartz into low-Ti quartz and acicular rutile. In our samples, rutile needles are generally restricted to grain cores and are consistent with quartz crystallographic orientations, which strongly proves the second mechanism (Storm and Spear, 2009; Thomas and Nachlas, 2020). The dark "spots" in the CL images observed by Cherniak et al. (2007) were also interpreted as the feature of rutile exsolution during the post-peak cooling.

For both quartz inclusions and matrix-type quartz, especially the latter without garnet protection, some grains contain low Ti concentrations, which suggest the occurrence of later resetting. Healed fracture structures exist in both quartz inclusions and matrix-type quartz, which are similar to filled fractures in plutonic quartz and fluid-controlled quartz recovery in granulites (Seyedolali

et al., 1997; Van den Kerkhof et al., 2004). Quartz first formed with non-healed fractures owing to the stresses imposed on the grains and decrepitation of fluid inclusions caused by the pressure difference between fluid inclusions and host quartz, probably by tectonic settings, such as uplift. Subsequently, the fractures were filled with secondary quartz or quartz nuclei by precipitation of non-luminescing SiO_2. Quartz with such structures commonly contains high Ti concentrations and yields high TitaniQ temperatures. Thus, we propose that quartz with such fractures within our samples grew or recrystallized during post-peak nearly isothermal decompression.

The occurrence of reticular structure in quartz is less common in our samples, and quartz with such structures contains relatively low Ti concentrations and accordingly records low TitaniQ temperatures. Many studies have verified a positive correlation between Ti concentrations in quartz and CL intensity (Sprunt et al., 1978; Müller et al., 2002; Spear and Wark, 2009). Thus, the Ti concentrations are heterogeneously distributed. Reticular zoning might indicate the pathway of fluid infiltration.

In summary, we posit that matrix-type quartz with extensive rutile exsolution most probably grew during the near-peak to the early cooling stage and can better constrain the near-peak conditions of the studied samples than inclusion-type quartz. Therefore, the variation in the maximum TitaniQ temperatures of matrix-type quartz in these samples can better show the thermal regime of the studied region.

Validity of the TitaniQ Thermometer

Another major question can be posed to interpret the meaning of TitaniQ temperature: *Can the matrix-type quartz that formed*
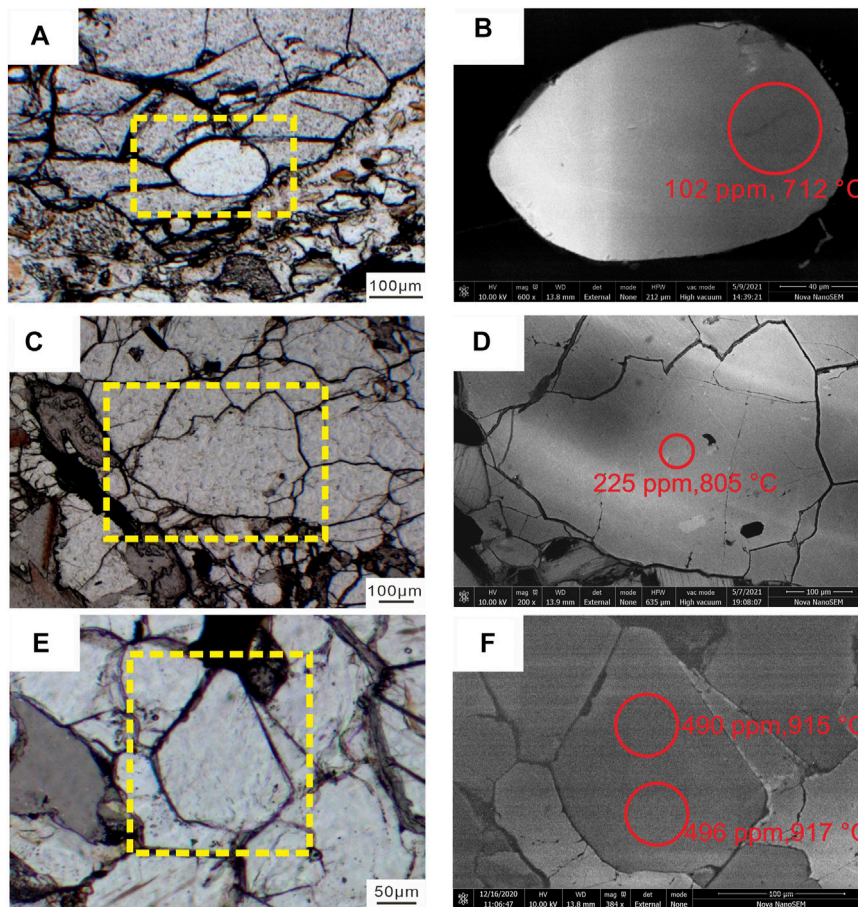
FIGURE 6 | Representative photomicrographs and CL images of the analyzed quartz grains showing non-structure with homogeneous luminescence. **(A)** Quartz inclusion within garnet rim in sample 20HL101, and CL image is shown in **(B)**; **(C,E)** Matrix-type quartz in samples 09XH07 and 09JGQ15, and CL images are shown in **(D,F)**, respectively. The red circle marks the analyzed EPMA spot.

during near-peak or early cooling preserve the original Ti concentrations? Mechanisms for quartz Ti re-equilibrium are diffusion (e.g., both lattice and grain boundary diffusion) and recrystallization during deformation and/or retrogression.

Experimental studies have shown that Ti diffusion is slow in quartz (Cherniak et al., 2007; Jollands et al., 2020). According to Cherniak et al. (2007), the diffusion distance of Ti-in-quartz is 0.05, 2, and 5 μm at 0.001, 1.0, and 10 Ma at 500°C. However, the diffusion distances increased to 16 μm, 500 μm, and 1,600 μm over the same time range at 800°C. Nevertheless, experiments under anhydrous conditions suggest that grain boundary diffusion is 3–4 orders of magnitude faster than lattice diffusion (Bromiley and Hiscock, 2016). Therefore, the grain boundary acts as an efficient conduit for Ti equilibrium, especially in fine-grained rocks. Studies have shown an increasing trend of Ti concentrations from the core toward the rim in quartz inclusions of garnet, interpreted as an exchange with the host garnet (Spear et al., 2012), but we did not recognize such features in our samples.

Many studies have suggested that dynamic recrystallization is an efficient mechanism for Ti re-equilibrium, especially fast grain boundary migration, which is crucial for Ti re-equilibrium at high

temperatures (Stipp et al., 2002; Grujic et al., 2011). Generally, recrystallized quartz, which has well-developed facets impinging on the preliminary quartz, results in cuspate, serrated, and irregular grain boundaries of preliminary quartz (Thomas and Nachlas, 2020). Typical serrated boundaries from matrix-type quartz shown in **Figures 5C,D** suggest incomplete re-equilibration and would contain low Ti concentrations; thus, we did not select domains near the serrated boundaries for analysis.

Despite the aforementioned factors, the highest TitaniQ temperatures (ca. 960–970°C) are broadly consistent with the reported temperatures calculated by other methods in the studied region (Santosh et al., 2007a; Jiao et al., 2013a; Jiao et al., 2013b; Li and Wei, 2016; Li and Wei, 2018), for example, 966–1,096°C by a two-feldspar thermometer in Xuwujia, 850–1,000°C by a Zr-in-rutile thermometer in Tuiguishan, 940–1,030°C by Ti-in-zircon and a ternary feldspar thermometer in Nantianmen and Xiaonangou, ~975°C based on phase equilibria modeling in Xumayao, and 930–1,050°C by pseudosection in Hongsigou (Jiao et al., 2011; Jiao and Guo, 2011; Liu et al., 2012; Zhang et al., 2012; Yang et al., 2014). This result confirms the validity of the TitaniQ thermometer in
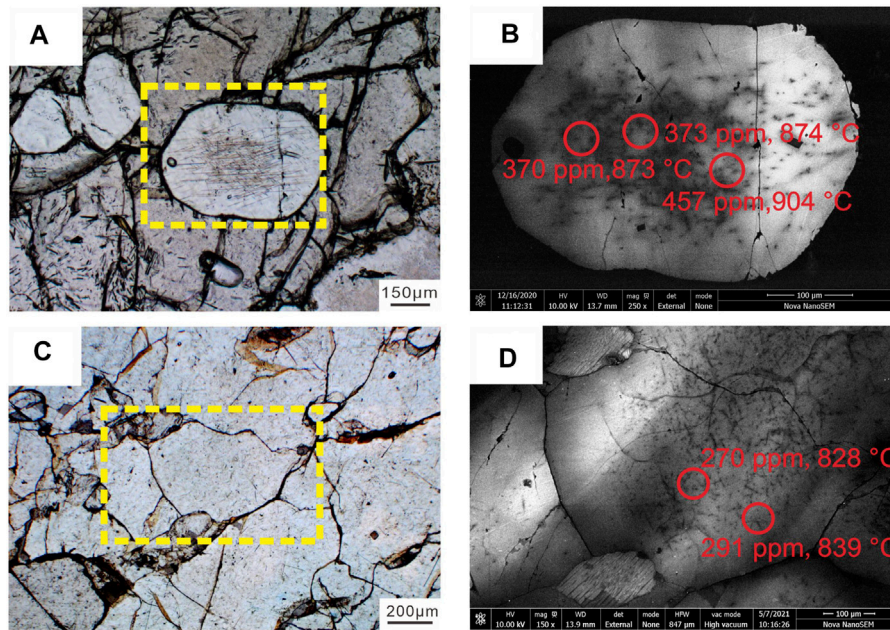
FIGURE 7 | Representative photomicrographs and CL images of the analyzed quartz grains showing linear structure with low luminescence. **(A)** Quartz inclusion within garnet in sample 09JGQ15 and CL image is shown in **(B)**; **(C)** Matrix-type quartz in sample 09DSZ17 and CL image is shown in **(D)**.
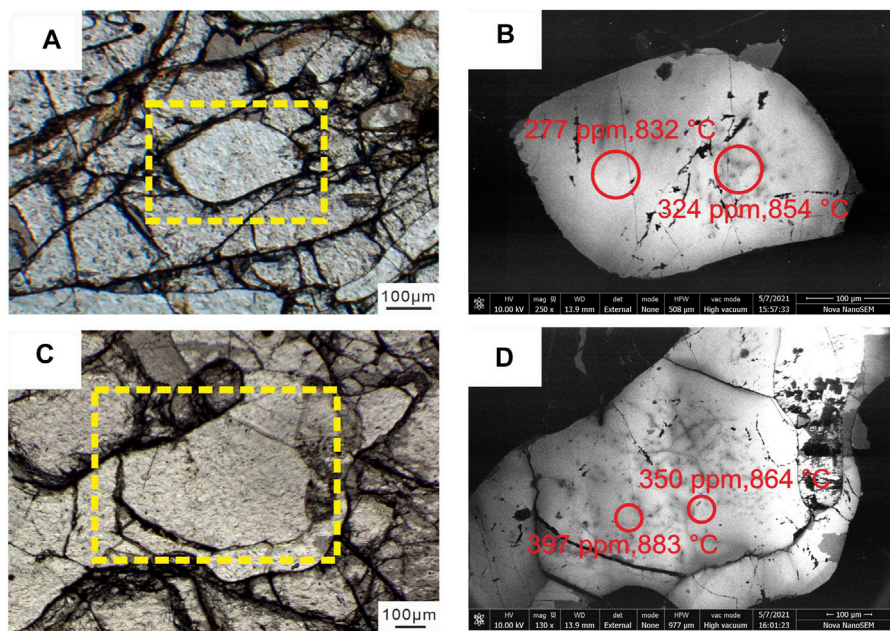

FIGURE 8 | Representative photomicrographs and CL images of the analyzed quartz grains showing healed fractures. **(A,C)** Quartz inclusion within garnet and matrix-type quartz both in sample 09DSZ35, and CL image is shown in **(B,D)**, respectively.

high-grade rocks, and TitaniQ temperatures may represent the minimum estimates of the peak temperatures.

Other possible influences on our calculated temperatures were 1) the pressure estimation, 2) the location of selected analytical spots, and 3) sample bias. We set a pressure of 8 kbar for all calculations in this study. Pressure at 1 kbar higher would result in a 30°C higher calculated temperature. The analyzed domains with abundant rutile needles contain higher Ti concentrations
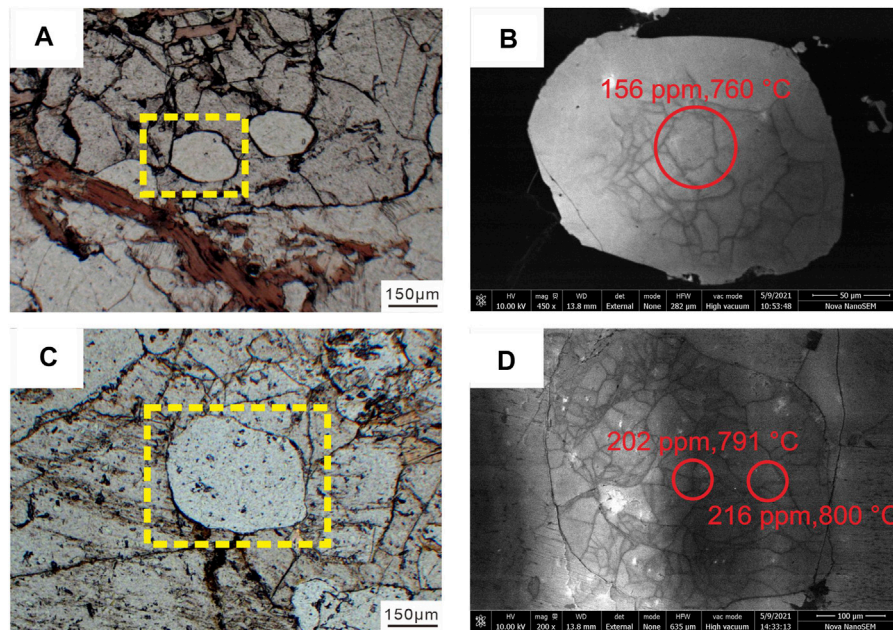
FIGURE 9 | Representative photomicrographs and CL images of the analyzed quartz grains showing reticular structure. **(A)** Quartz inclusion within garnet in sample 20HL59 and CL image is shown in **(B)**; **(C)** Matrix-type quartz in sample 20HL89 and CL image is shown in **(D)**.

than the domains without rutile needles; therefore, if any, we generally selected domains with the most abundant rutile needles for analysis. However, quartz and rutile have different crystal structure, which result in different characteristic X-ray efficiencies. This effect might influence the measured Ti concentrations. The EMP analytical spots are actually in two-dimension, which may underestimate the real volume percentage of rutile needles in quartz. Finally, we must acknowledge that in some samples we probably missed the quartz grain that contains the highest Ti concentrations, and in this case, the maximum TitaniQ temperatures for such samples would be underestimated.

Thermal Regime of the Eastern Khondalite Belt

In **Figure 10A**, the mapping is based on the temperature calculated from the maximum Ti concentrations of matrix-type quartz in each sample; for comparison, that in **Figure 10B** is based on the temperature calculated from the average Ti concentrations of matrix-type quartz in each sample. Sample localities are marked in the picture to show the distribution of the samples and the effect of sample bias.
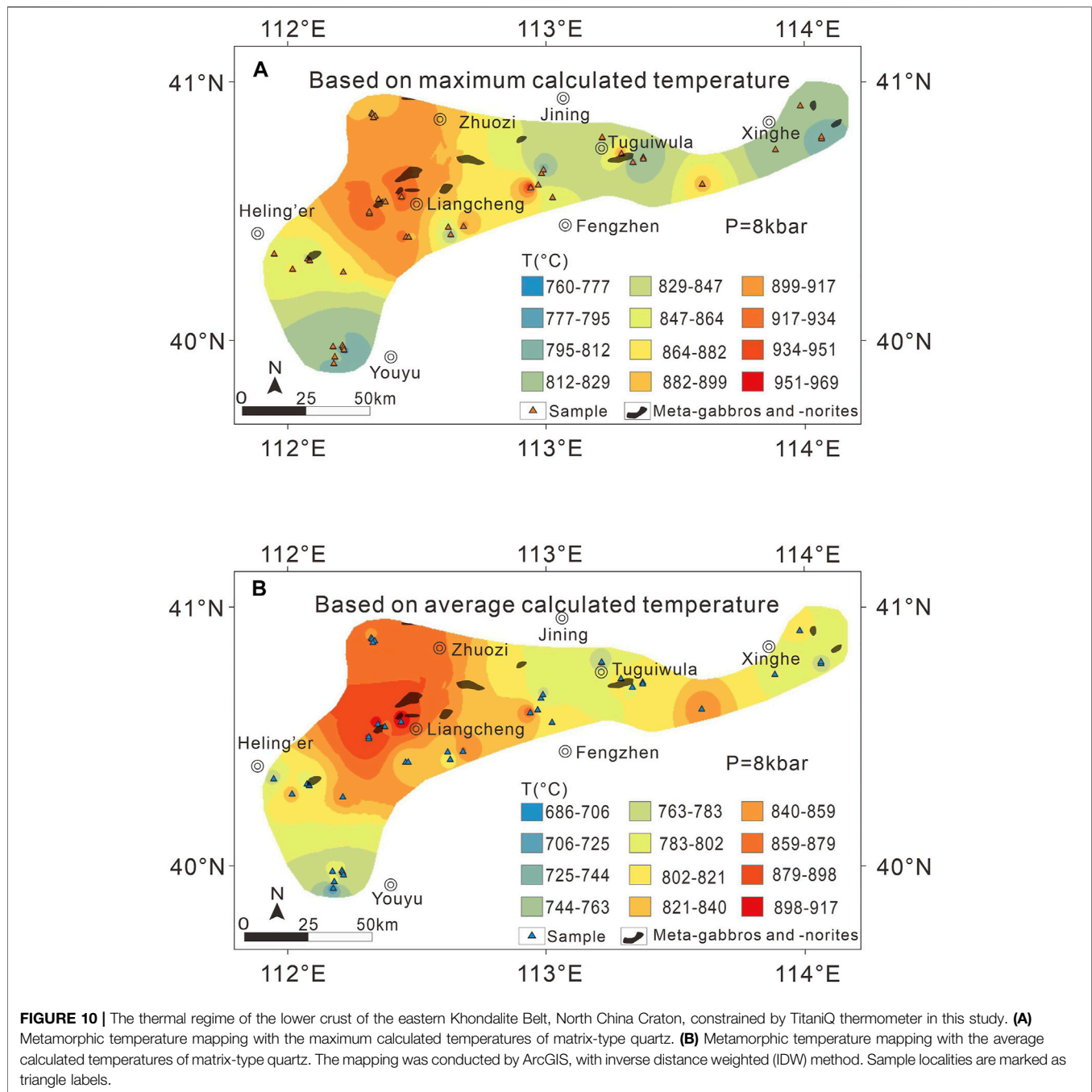
Both temperature mapping results show that the large-scale and extremely hot regions are surrounded by Liangcheng, Heling'er, and Zhuozi. The maximum TitaniQ temperatures were >900°C, suggesting the occurrence of UHT metamorphism. This phenomenon is consistent with those of several UHT metamorphic localities reported in this area (e.g., Liu et al., 2012; Jiao et al., 2013a; Jiao et al., 2013b). This hottest area was also consistent with the region where extensive charnockite occurred (**Figure 1**). Our results also show that

Tuguiwula area, where typical UHT granulites with diagnostic Spr + Qz and Opx + Sil + Qz mineral assemblages have been reported, are hot, but the scale of the hot region is limited and surrounded by a relatively cold region. It might imply that the surrounding area is probably located at a higher crustal level. Alternatively, it is noticed that we have not collected samples from Zhuozi to Jining and further to Tuguiwula because of the thick sediment cover. The variation of temperatures in this region is probably caused by sample bias. Therefore, it is also possible that the whole area of Heling'er-Liangcheng-Tuguiwula-Jining-Zhuozi have experienced UHT metamorphism. It requires confirmation in future research.

In contrast, the Youyu and Xinghe areas are not as hot as the Liangcheng-Heling'er-Zhuozi area, although the major mineral assemblages are mostly the same. The maximum TitaniQ temperature is below 900°C, implying that these two areas probably do not experience UHT metamorphism. Alternatively, the analyzed quartz probably crystallized during the later stage of post-peak cooling. Quartz from these areas generally shows a non-structure with homogeneous luminescence structures, and rutile needles cannot be observed.

The thermal regime of the eastern Khondalite Belt, established by the TitaniQ thermometer in this case, is consistent with the results of another independent study using Zr-in-rutile thermometry mapping (Qi et al., unpublished). This particular case study further confirms the validity of the TitaniQ thermometer in recognizing UHT metamorphism and constraining its thermal conditions and spatial scales.

Several models have been proposed to interpret the formation of UHT metamorphism in the eastern Khondalite Belt, including radiogenic heat production (Jiao et al., 2013a), post-collisional

FIGURE 10 | The thermal regime of the lower crust of the eastern Khondalite Belt, North China Craton, constrained by TitaniQ thermometer in this study. (A) Metamorphic temperature mapping with the maximum calculated temperatures of matrix-type quartz. (B) Metamorphic temperature mapping with the average calculated temperatures of matrix-type quartz. The mapping was conducted by ArcGIS, with inverse distance weighted (IDW) method. Sample localities are marked as triangle labels.

lithosphere extension due to asthenospheric upwelling (Zhao, 2009; Li and Wei, 2018; Jiao et al., 2021), ridge subduction (Santosh and Kusky, 2009; Peng et al., 2011; Santosh et al., 2012), mantle plume (Santosh et al., 2008), and emplacement of mantle-derived mafic magma (Huang et al., 2019). In addition, a back-arc setting has also been proposed to explain UHT metamorphism in other regions (Brown, 2006; Brown and Johnson, 2018). Our study certifies the regional distribution of UHT metamorphism in the eastern Khondalite Belt, and the large-scale hottest region is the Liangcheng-Heling'er-Zhuozi

area, which is consistent with the occurrence of extensive charnockite. This result implies that the formation of UHT metamorphism is closely related to charnockite. This extremely hot metamorphism and magmatism might be the coupling effect of the same mechanism, which probably formed in the root of a Paleoproterozoic large hot orogeny. However, we could not distinguish these UHT formation models in this study, and the potential model should be able to explain the spatially close relationship between UHT metamorphism and charnockite.

CONCLUSION

In this study, we first applied TitaniQ thermometer to 44 aluminous gneisses/granulites in the Paleoproterozoic eastern Khondalite Belt, collected from an area of ~10,000 km². Our results show that matrix-type quartz with substantial rutile exsolution generally yielded the maximum TitaniQ temperatures, and that of quartz inclusions in garnet was <160°C lower. These results implied that quartz inclusions probably formed during the prograde metamorphism, and matrix-type rutile needle-rich quartz formed during the near-peak to early cooling stages. The temperature mapping result based on the maximum TitaniQ temperatures of matrix-type quartz indicates that the hottest Paleoproterozoic lower crust is beneath the Liangcheng-Heling'er-Zhuozi area, where UHT metamorphism is closely associated with abundant charnockite. This region may represent the root of an ancient large hot orogeny.

DATA AVAILABILITY STATEMENT

The original contributions presented in the study are included in the article/**Supplementary Material**, further inquiries can be directed to the corresponding author.

REFERENCES

AUTHOR CONTRIBUTIONS

SJ designed the research plan. SJ, YQ, and YZ went to the fieldtrip and collected the samples. DZ and YZ analyzed the samples. YZ wrote the original manuscript. All authors revised the manuscript.

SUPPLEMENTARY MATERIAL

The Supplementary Material for this article can be found online at: https://www.frontiersin.org/articles/10.3389/feart.2022.860057/full#supplementary-material

Acosta, M. D., Watkins, J. M., Reed, M. H., Donovan, J. J., and DePaolo, D. J. (2020). Ti-in-quartz: Evaluating the Role of Kinetics in High Temperature crystal Growth Experiments. *Geochimica et Cosmochimica Acta* 281, 149–167. doi:10.1016/j.gca.2020.04.030

Audétat, A., Garbe-Schönberg, D., Kronz, A., Pettke, T., Rusk, B., Donovan, J. J., et al. (2015). Characterisation of a Natural Quartz crystal as a Reference Material for Microanalytical Determination of Ti, Al, Li, Fe, Mn, Ga and Ge. *Geostand Geoanal Res.* 39 (2), 171–184. doi:10.1111/j.1751-908X.2014.00309.x

Bromiley, G. D., and Hiscock, M. (2016). Grain Boundary Diffusion of Titanium in Polycrystalline Quartz and its Implications for Titanium in Quartz (TitaniQ) Geothermobarometry. *Geochimica et Cosmochimica Acta* 178, 281–290. doi:10.1016/j.gca.2016.01.024

Brown, M. (2006). Duality of thermal Regimes Is the Distinctive Characteristic of Plate Tectonics since the Neoarchean. *Geol.* 34 (11), 961–964. doi:10.1130/G22853A.1

Brown, M., and Johnson, T. (2018). Secular Change in Metamorphism and the Onset of Global Plate Tectonics. *Am. Mineral.* 103 (2), 181–196. doi:10.2138/am-2018-6166

Cherniak, D. J., Watson, E. B., and Wark, D. A. (2007). Ti Diffusion in Quartz. *Chem. Geology* 236 (1–2), 65–74. doi:10.1016/j.chemgeo.2006.09.001

Dan, W., Li, X.-H., Guo, J., Liu, Y., and Wang, X.-C. (2012). Integrated *In Situ* Zircon U-Pb Age and Hf-O Isotopes for the Helanshan Khondalites in North China Craton: Juvenile Crustal Materials Deposited in Active or Passive continental Margin? *Precambrian Res.* 222-223, 143–158. doi:10.1016/j.precamres.2011.07.016

Geng, Y., Du, L., and Ren, L. (2012). Growth and Reworking of the Early Precambrian continental Crust in the North China Craton: Constraints from Zircon Hf Isotopes. *Gondwana Res.* 21, 517–529. doi:10.1016/j.gr.2011.07.006

Ghent, E. D., and Stout, M. Z. (1984). TiO2 Activity in Metamorphosed Pelitic and Basic Rocks: Principles and Applications to Metamorphism in southeastern Canadian Cordillera. *Contr. Mineral. Petrol.* 86 (3), 248–255. doi:10.1007/BF00373670

Gou, L., Li, Z., Liu, X., Dong, Y., Zhao, J., Zhang, C., et al. (2018). Ultrahigh-temperature Metamorphism in the Helanshan Complex of the Khondalite Belt, North China Craton: Petrology and Phase Equilibria of Spinel-Bearing Pelitic Granulites. *J. Metamorph Geol.* 36, 1199. doi:10.1111/jmg.12442

Grujic, D., Stipp, M., and Wooden, J. (2011). Thermometry of Quartz Mylonites: Importance of Dynamic Recrystallization on Ti-in-quartz Reequilibration. *Geochem. Geophys. Geosys.* 12. doi:10.1029/2010GC003368

Guo, J., Peng, P., Chen, Y., Jiao, S., and Windley, B. F. (2012). UHT Sapphirine Granulite Metamorphism at 1.93-1.92Ga Caused by Gabbronorite Intrusions: Implications for Tectonic Evolution of the Northern Margin of the North China Craton. *Precambrian Res.* 222-223, 124–142. doi:10.1016/j.precamres.2011.07.020

Harley, S. L. (1998). On the Occurrence and Characterization of Ultrahigh-Temperature Crustal Metamorphism. *Geol. Soc. Lond. Spec. Publications* 138, 81–107. doi:10.1144/GSL.SP.1996.138.01.06

Harley, S. L. (2008). Refining the P-T Records of UHT Crustal Metamorphism. *J. Metamorph Geol.* 26, 125–154. doi:10.1111/j.1525-1314.2008.00765.x

Hayden, L. A., and Watson, E. B. (2007). Rutile Saturation in Hydrous Siliceous Melts and its Bearing on Ti-Thermometry of Quartz and Zircon. *Earth Planet. Sci. Lett.* 258 (3–4), 561–568. doi:10.1016/j.epsl.2007.04.020

Hildreth, W., and Wilson, C. J. N. (2007). Compositional Zoning of the Bishop Tuff. *J. Petrol.* 48 (5), 951–999. doi:10.1093/petrology/egm007

Huang, G., Guo, J., Jiao, S., and Palin, R. (2019). What Drives the Continental Crust to Be Extremely Hot So Quickly? *J. Geophys. Res. Solid Earth* 124 (11), 11218–11231. doi:10.1029/2019JB017840

Huang, R., and Audétat, A. (2012). The Titanium-In-Quartz (TitaniQ) Thermobarometer: A Critical Examination and Re-calibration. *Geochimica et Cosmochimica Acta* 84, 75–89. doi:10.1016/j.gca.2012.01.009

Jiang, X., Yu, S., Liu, Y., Li, S., Lv, P., Peng, Y., et al. (2022). Episodic Metamorphism and Anatexis within the Khondakite Belt, North China Craton: Constraint from Late-Paleoproterozoic Fluid-Fluxed Melting of the Daqingshan Complex. *Precambrian Res.* 369, 106504. doi:10.1016/j.precamres.2021.106504

Jiao, S.-J., Guo, J.-H., Wang, L.-J., and Peng, P. (2015). Short-lived High-Temperature Prograde and Retrograde Metamorphism in Shaerqin Sapphirine-Bearing Metapelites from the Daqingshan Terrane, North China Craton. *Precambrian Res.* 269, 31–57. doi:10.1016/j.precamres.2015.08.002

Jiao, S., Evans, N. J., Guo, J., Fitzsimons, I. C. W., Zi, J.-W., and McDonald, B. J. (2021). Establishing the P-T Path of UHT Granulites by Geochemically Distinguishing Peritectic from Retrograde Garnet. *Am. Mineral.* 106, 1640–1653. doi:10.2138/am-2021-7681

Jiao, S., Fitzsimons, I. C. W., Zi, J.-W., Evans, N. J., Mcdonald, B. J., and Guo, J. (2020). Texturally Controlled U-Th-Pb Monazite Geochronology Reveals Paleoproterozoic UHT Metamorphic Evolution in the Khondalite Belt, North China Craton. *J. Petrol.* 61 (1), egaa023. doi:10.1093/petrology/egaa023

Jiao, S., and Guo, J. (2011). Application of the Two-Feldspar Geothermometer to Ultrahigh-Temperature (UHT) Rocks in the Khondalite belt, North China Craton and its Implications. *Am. Mineral.* 96 (2–3), 250–260. doi:10.2138/am.2011.3500

Jiao, S., Guo, J., Harley, S. L., and Peng, P. (2013a). Geochronology and Trace Element Geochemistry of Zircon, Monazite and Garnet from the Garnetite And/or Associated Other High-Grade Rocks: Implications for Palaeoproterozoic Tectonothermal Evolution of the Khondalite Belt, North China Craton. *Precambrian Res.* 237, 78–100. doi:10.1016/j.precamres.2013.09.008

Jiao, S., Guo, J., Harley, S. L., and Windley, B. F. (2013b). New Constraints from Garnetite on the P-T Path of the Khondalite Belt: Implications for the Tectonic Evolution of the North China Craton. *J. Petrol.* 54 (9), 1725–1758. doi:10.1093/petrology/egt029

Jiao, S., Guo, J., Mao, Q., and Zhao, R. (2011). Application of Zr-In-Rutile Thermometry: a Case Study from Ultrahigh-Temperature Granulites of the Khondalite belt, North China Craton. *Contrib. Mineral. Petrol.* 162 (2), 379–393. doi:10.1007/s00410-010-0602-3

Jiao, S., and Guo, J. (2020). Paleoproterozoic UHT Metamorphism with Isobaric Cooling (IBC) Followed by Decompression-Heating in the Khondalite Belt (North China Craton): New Evidence from Two Sapphirine Formation Processes. *J. Metamorph Geol.* 38 (4), 357–378. doi:10.1111/jmg.12525

Jollands, M. C., Bloch, E., and Müntener, O. (2020). New Ti-in-Quartz Diffusivities Reconcile Natural Ti Zoning with Time Scales and Temperatures of Upper Crustal Magma Reservoirs. *Geology* 48, 654–657. doi:10.1130/G47238.1

Kendrick, J., and Indares, A. (2018). The Ti Record of Quartz in Anatectic Aluminous Granulites. *J. Petrol.* 59 (8), 1493–1516. doi:10.1093/petrology/egy070

Kidder, S., Avouac, J.-P., and Chan, Y.-C. (2013). Application of Titanium-In-Quartz Thermobarometry to Greenschist Facies Veins and Recrystallized Quartzites in the Hsüehshan Range, Taiwan. *Solid Earth* 4 (1), 1–21. doi:10.5194/se-4-1-2013

Kularatne, K., and Audétat, A. (2014). Rutile Solubility in Hydrous Rhyolite Melts at 750-900°C and 2kbar, with Application to Titanium-In-Quartz (TitaniQ) Thermobarometry. *Geochimica et Cosmochimica Acta* 125, 196–209. doi:10.1016/j.gca.2013.10.020

Li, X., and Wei, C. (2018). Ultrahigh-temperature Metamorphism in the Tuguiwula Area, Khondalite Belt, North China Craton. *J. Metamorph. Geol.* 36 (4), 489–509. doi:10.1111/jmg.12301

Li, X. W., and Wei, C. J. (2016). Phase Equilibria Modelling and Zircon Age Dating of Pelitic Granulites in Zhaojiayao, from the Jining Group of the Khondalite Belt, North China Craton. *J. Metamorph. Geol.* 34 (6), 595–615. doi:10.1111/jmg.12195

Liu, D. Y., Nutman, A. P., Compston, W., Wu, J. S., and Shen, Q. H. (1992). Remnants of ≥3800 Ma Crust in the Chinese Part of the Sino-Korean Craton. *Geol.* 20 (4), 339–342. doi:10.1130/0091-7613(1992)020<0339:romcit>2.3.co;2

Liu, S. J., Li, J. H., and Santosh, M. (2010). First Application of the Revised Ti-In-Zircon Geothermometer to Paleoproterozoic Ultrahigh-Temperature Granulites of Tuguiwula, Inner Mongolia, North China Craton. *Contrib. Mineral. Petrol.* 159 (2), 225–235. doi:10.1007/s00410-009-0425-2

Liu, S., Tsunogae, T., Li, W., Shimizu, H., Santosh, M., Wan, Y., et al. (2012). Paleoproterozoic Granulites from Heling'er: Implications for Regional Ultrahigh-Temperature Metamorphism in the North China Craton. *Lithos* 148, 54–70. doi:10.1016/j.lithos.2012.05.024

Merlet, C. (1994). An Accurate Computer Correction Program for Quantitative Electron Probe Microanalysis. *Mikrochim Acta* 114-115, 363–376. doi:10.1007/BF01244563

Müller, A., Lennox, P., and Trzebski, R. (2002). Cathodoluminescence and Micro-structural Evidence for Crystallisation and Deformation Processes of Granites

in the Eastern Lachlan Fold Belt (SE Australia). *Contrib. Mineral. Petrol.* 143 (4), 510–524. doi:10.1007/s00410-002-0361-x

Ostapenko, G. T., Gamarnik, M. Y., Gorogotskaya, L. I., Kuznetsov, G. V., Tarashchan, A. N., and Timoshkova, L. P. (1987). Isomorphism of Titanium Substitution for Silicon in Quartz: Experimental Data. *Mineral. Zh* 9, 30–40.

Peng, P., Guo, J.-H., Windley, B. F., and Li, X.-H. (2011). Halaqin Volcano-Sedimentary Succession in the central-northern Margin of the North China Craton: Products of Late Paleoproterozoic ridge Subduction. *Precambrian Res.* 187, 165–180. doi:10.1016/j.precamres.2011.03.006

Peng, P., Guo, J. H., Windley, B. F., Liu, F., Chu, Z., and Zhai, M. G. (2012). Petrogenesis of Late Paleoproterozoic Liangcheng Charnockites and S-type Granites in the central-northern Margin of the North China Craton: Implications for ridge Subduction. *Precambrian Res.* 222-223, 107–123. doi:10.1016/j.precamres.2011.06.002

Peng, P., Guo, J., Zhai, M., and Bleeker, W. (2010). Paleoproterozoic Gabbronoritic and Granitic Magmatism in the Northern Margin of the North China Craton: Evidence of Crust-Mantle Interaction. *Precambrian Res.* 183, 635–659. doi:10.1016/j.precamres.2010.08.015

Sajeev, K., Osanai, Y., and Santosh, M. (2004). Ultrahigh-temperature Metamorphism Followed by Two-Stage Decompression of Garnet-Orthopyroxene-Sillimanite Granulites from Ganguvarpatti, Madurai Block, Southern India. *Contrib. Mineral. Petrol.* 148 (1), 29–46. doi:10.1007/s00410-004-0592-0

Santosh, M., and Kusky, T. (2010). Origin of Paired High Pressure–ultrahigh-Temperature Orogens: a ridge Subduction and Slab Window Model. *Terra Nova* 22 (1), 35–42. doi:10.1111/j.1365-3121.2009.00914.x

Santosh, M., Liu, S. J., Tsunogae, T., and Li, J. H. (2012). Paleoproterozoic Ultrahigh-Temperature Granulites in the North China Craton: Implications for Tectonic Models on Extreme Crustal Metamorphism. *Precambrian Res.* 222-223 (223), 77–106. doi:10.1016/j.precamres.2011.05.003

Santosh, M., Sajeev, K., Li, J. H., and Liu, S. J. (2006). Extreme Crustal Metamorphism during Columbia Supercontinent Assembly: Evidence from North China Craton. *Gondwana Res.* 10 (3–4), 256–266. doi:10.1016/j.gr.2006.06.005

Santosh, M., Tsunogae, T., Li, J. H., and Liu, S. J. (2007a). Discovery of Sapphirine-Bearing Mg-Al Granulites in the North China Craton: Implications for Paleoproterozoic Ultrahigh Temperature Metamorphism. *Gondwana Res.* 11 (3), 263–285. doi:10.1016/j.gr.2006.10.009

Santosh, M., Tsunogae, T., Ohyama, H., Sato, K., Li, J. H., and Liu, S. J. (2008). Carbonic Metamorphism at Ultrahigh-Temperatures: Evidence from North China Craton. *Earth Planet. Sci. Lett.* 266 (1–2), 149–165. doi:10.1016/j.epsl.2007.10.058

Santosh, M., Wan, Y., Liu, D., Chunyan, D., and Li, J. (2009). Anatomy of Zircons from an Ultrahot Orogen: the Amalgamation of the North China Craton within the Supercontinent Columbia. *J. Geology* 117 (4), 429–443. doi:10.1086/598949

Santosh, M., Wilde, S., and Li, J. (2007b). Timing of Paleoproterozoic Ultrahigh-Temperature Metamorphism in the North China Craton: Evidence from SHRIMP U-Pb Zircon Geochronology. *Precambrian Res.* 159 (3–4), 178–196. doi:10.1016/j.precamres.2007.06.006

Sato, K., and Santosh, M. (2007). Titanium in Quartz as a Record of Ultrahigh-Temperature Metamorphism: the Granulites of Karur, Southern India. *Mineral. Mag.* 71 (2), 143–154. doi:10.1180/minmag.2007.071.2.143

Seyedolali, A., Krinsley, D. H., Boggs, S., Jr., O'Hara, P. F., Dypvik, H., and Goles, G. G. (1997). Provenance Interpretation of Quartz by Scanning Electron Microscope–Cathodoluminescence Fabric Analysis. *Geology* 25, 787–790. doi:10.1130/0091-7613(1997)025<0787:PIOQBS>2.3.CO;2

Shazia, J. R., Santosh, M., and Sajeev, K. (2012). Peraluminous Sapphirine-Cordierite Pods in Mg-Rich Orthopyroxene Granulite from Southern India: Implications for Lower Crustal Processes. *J. Asian Earth Sci.* 58, 88–97. doi:10.1016/j.jseaes.2012.06.020

Spear, F. S., Ashley, K. T., Webb, L. E., and Thomas, J. B. (2012). Ti Diffusion in Quartz Inclusions: Implications for Metamorphic Time Scales. *Contrib. Mineral. Petrol.* 164 (6), 977–986. doi:10.1007/s00410-012-0783-z

Spear, F. S., and Wark, D. A. (2009). Cathodoluminescence Imaging and Titanium Thermometry in Metamorphic Quartz. *J. Metamorphic Geology* 27 (3), 187–205. doi:10.1111/j.1525-1314.2009.00813.x

Sprunt, E. S., Dengler, L. A., and Sloan, D. (1978). Effects of Metamorphism on Quartz Cathodoluminescence. *Geol.* 6 (5), 305–308. doi:10.1130/0091-7613(1978)6<305:eomoqc>2.0.co;2

Stipp, M., Stünitz, H., Heilbronner, R., and Schmid, S. M. (2002). Dynamic Recrystallization of Quartz: Correlation between Natural and Experimental Conditions. *Geol. Soc. Lond. Spec. Publications* 200, 171–190. doi:10.1144/GSL.SP.2001.200.01.11

Storm, L. C., and Spear, F. S. (2009). Application of the Titanium-In-Quartz Thermometer to Pelitic Migmatites from the Adirondack Highlands, New York. *J. Metamorphic Geology* 27 (7), 479–494. doi:10.1111/j.1525-1314.2009.00829.x

Thomas, J. B., and Bruce Watson, E. (2012). Application of the Ti-in-quartz thermobarometer to rutile-free systems. Reply to: a comment on on: 'TitaniQ under pressure: the effect of pressure and temperature on the solubility of Ti in quartz' by Thomas et al. *Contrib. Mineral. Petrol.* 164 (2), 369–374. doi:10.1007/s00410-012-0761-5

Thomas, J. B., Bruce Watson, E., Spear, F. S., Shemella, P. T., and Lanzirotti, S. K. A. (2010). TitaniQ under Pressure: the Effect of Pressure and Temperature on the Solubility of Ti in Quartz. *Contrib. Mineral. Petrol.* 160 (5), 743–759. doi:10.1007/s00410-010-0505-3

Thomas, J. B., and Nachlas, W. O. (2020). Discontinuous Precipitation of Rutilated Quartz: Grain-Boundary Migration Induced by Changes to the Equilibrium Solubility of Ti in Quartz. *Contrib. Mineral. Petrol.* 175 (4), 38. doi:10.1007/s00410-020-01676-2

Thomas, J. B., Watson, E. B., Spear, F. S., and Wark, D. A. (2015). TitaniQ Recrystallized: Experimental Confirmation of the Original Ti-in-Quartz Calibrations. *Contrib. Mineral. Petrol.* 169 (3), 27. doi:10.1007/s00410-015-1120-0

Tual, L., Möller, C., and Whitehouse, M. J. (2018). Tracking the Prograde P-T Path of Precambrian Eclogite Using Ti-in-Quartz and Zr-In-Rutile Geothermobarometry. *Contrib. Mineral. Petrol.* 173 (7), 56. doi:10.1007/s00410-018-1482-1

Van den Kerkhof, A. M., Kronz, A., Simon, K., and Scherer, T. (2004). Fluid-Controlled Quartz Recovery in Granulite as Revealed by Cathodoluminescence and Trace Element Analysis (Bamble Sector, Norway). *Contrib. Mineral. Petrol.* 146 (5), 637–652. doi:10.1007/s00410-003-0523-5

Wan, Y., Liu, D., Dong, C., Xu, Z., Wang, Z., Wilde, S. A., et al. (2009). The Precambrian Khondalite Belt in the Daqingshan Area, North China Craton: Evidence for Multiple Metamorphic Events in the Palaeoproterozoic Era. *Geol. Soc. Lond. Spec. Publications* 323, 73–97. doi:10.1144/SP323.4

Wan, Y., Liu, D., Song, B., Wu, J., Yang, C., Zhang, Z., et al. (2005). Geochemical and Nd Isotopic Compositions of 3.8Ga Meta-Quartz Dioritic and Trondhjemitic Rocks from the Anshan Area and Their Geological Significance. *J. Asian Earth Sci.* 24, 563–575. doi:10.1016/j.jseaes.2004.02.009

Wang, B., Wei, C.-J., Tian, W., and Fu, B. (2020). UHT Metamorphism Peaking Above 1100 °C with Slow Cooling: Insights from Pelitic Granulites in the Jining Complex, North China Craton. *J. Petrol.* 61, egaa070. doi:10.1093/petrology/egaa070

Wang, L.-J., Guo, J.-H., Yin, C., and Peng, P. (2017). Petrogenesis of Ca. 1.95 Ga Meta-Leucogranites from the Jining Complex in the Khondalite Belt, North China Craton: Water-Fluxed Melting of Metasedimentary Rocks. *Precambrian Res.* 303, 355–371. doi:10.1016/J.PRECAMRES.2017.04.036

Wang, L.-J., Guo, J.-H., Yin, C., Peng, P., Zhang, J., Spencer, C. J., et al. (2018). High-temperature S-type Granitoids (Charnockites) in the Jining Complex, North China Craton: Restite Entrainment and Hybridization with Mafic Magma. *Lithos* 320-321, 435–453. doi:10.1016/j.lithos.2018.09.035

Wark, D. A., and Watson, E. B. (2006). TitaniQ: a Titanium-In-Quartz Geothermometer. *Contrib. Mineral. Petrol.* 152 (6), 743–754. doi:10.1007/s00410-006-0132-1

Warr, L. N. (2021). Thousands of New and Improved mineral Symbols. *Nature* 598 (7882), 566. doi:10.1038/d41586-021-02884-x

Wu, F., Zhao, G., Wilde, S. A., and Sun, D. (2005). Nd Isotopic Constraints on Crustal Formation in the North China Craton. *J. Asian Earth Sci.* 24 (5), 523–545. doi:10.1016/j.jseaes.2003.10.011

Yang, Q.-Y., Santosh, M., and Tsunogae, T. (2014). Ultrahigh-temperature Metamorphism under Isobaric Heating: New Evidence from the North China Craton. *J. Asian Earth Sci.* 95, 2–16. doi:10.1016/j.jseaes.2014.01.018

Yin, C., Zhao, G., Guo, J., Sun, M., Xia, X., Zhou, X., et al. (2011). U-pb and Hf Isotopic Study of Zircons of the Helanshan Complex: Constrains on the Evolution of the Khondalite Belt in the Western Block of the North China Craton. *Lithos* 122 (1–2), 25–38. doi:10.1016/j.lithos.2010.11.010

Yin, C., Zhao, G., and Sun, M. (2015). High-pressure Pelitic Granulites from the Helanshan Complex in the Khondalite Belt, North China Craton: Metamorphic P-T Path and Tectonic Implications. *Am. J. Sci.* 315, 846–879. doi:10.2475/09.2015.03

Yin, C., Zhao, G., Sun, M., Xia, X., Wei, C., Zhou, X., et al. (2009). LA-ICP-MS U-Pb Zircon Ages of the Qianlishan Complex: Constrains on the Evolution of the Khondalite Belt in the Western Block of the North China Craton. *Precambrian Res.* 174, 78–94. doi:10.1016/j.precamres.2009.06.008

Zhai, M., and Peng, P. (2007). Paleoproterozoic Events in the North China Craton. *Acta Petrologica Sinica* 23, 2665–2682. (In Chinese with English Abstract).

Zhai, M. (2009). Two Kinds of Granulites (HT-HP and HT-UHT) in North China Craton: Their Genetic Relation and Geotectonic Implications. *Acta Petrologica Sinica* 25, 1753–1771. (In Chinese with English Abstract).

Zhang, C., Li, X., Almeev, R. R., Horn, I., Behrens, H., and Holtz, F. (2020). Ti-in-quartz Thermobarometry and TiO2 Solubility in Rhyolitic Melts: New Experiments and Parametrization. *Earth Planet. Sci. Lett.* 538, 116213. doi:10.1016/j.epsl.2020.116213

Zhang, H., Li, J., Liu, S., Li, W., Santosh, M., and Wang, H. (2012). Spinel + Quartz-Bearing Ultrahigh-Temperature Granulites from Xumayao, Inner Mongolia Suture Zone, North China Craton: Petrology, Phase Equilibria and Counterclockwise *P-T* Path. *Geosci. Front.* 3, 603–611. doi:10.1016/j.gsf.2012.01.003

Zhao, G., Li, S., Sun, M., and Wilde, S. A. (2011). Assembly, Accretion, and Break-Up of the Palaeo-Mesoproterozoic Columbia Supercontinent: Record in the North China Craton Revisited. *Int. Geology Rev.* 53 (11–12), 1331–1356. doi:10.1080/00206814.2010.527631

Zhao, G. (2009). Metamorphic Evolution of Major Tectonic Units in the Basement of the North China Craton: Key Issues and Discussion. *Acta Petrologica Sinica* 25, 1772–1792. (In Chinese with English Abstract).

Zhao, G., Sun, M., Wilde, S. A., and Li, S. (2003). Assembly, Accretion and Breakup of the Paleo-Mesoproterozoic Columbia Supercontinent: Records in the North China Craton. *Gondwana Res.* 6 (3), 417–434. doi:10.1016/S1342-937X(05)70996-5

Zhao, G., Sun, M., Wilde, S. A., and Sanzhong, L. (2005). Late Archean to Paleoproterozoic Evolution of the North China Craton: Key Issues Revisited. *Precambrian Res.* 136 (2), 177–202. doi:10.1016/j.precamres.2004.10.002

Zhao, G., Wilde, S. A., Cawood, P. A., and Lu, L. (1998). Thermal Evolution of Archean Basement Rocks from the Eastern Part of the North China Craton and its Bearing on Tectonic Setting. *Int. Geology Rev.* 40, 706–721. doi:10.1080/00206819809465233

Zhao, G., Wilde, S. A., Cawood, P. A., and Sun, M. (2001). Archean Blocks and Their Boundaries in the North China Craton: Lithological, Geochemical, Structural and P-T Path Constraints and Tectonic Evolution. *Precambrian Res.* 107 (1–2), 45–73. doi:10.1016/S0301-9268(00)00154-6

Zhou, X., Zhao, G., and Geng, Y. (2010). Helanshan High Pressure Politic Granulite: Petrologic Evidence for Collision Event in the Western Block of the North China Craton. *Acta Petrologica Sinica* 26, 2113–2121. (In Chinese with English abstract).